Journal of Biomechanics 84 (2019) 218–226

Contents lists available at ScienceDirect

Journal of Biomechanics

journal homepage: www.elsevier.com/locate/jbiomech
www.JBiomech.com

Modeling mitral valve stenosis: A parametric study on the stenosis severity level

Valentina Meschini [a], Francesco Viola [b,*], Roberto Verzicco [b,c]

[a] Gran Sasso Science Institute, Italy
[b] PoF Group, University of Twente, the Netherlands
[c] Department of Industrial Engineering, University of Roma Tor Vergata, Italy

ARTICLE INFO

Article history:
Accepted 2 January 2019

Keywords:
Mitral valve stenosis
Hemodynamics
Multi-physics model

ABSTRACT

New computational techniques providing more accurate representation of human heart pathologies could help uncovering relevant physical phenomena and improve the outcome of medical therapies. In this framework, the present work describes an efficient computational model for the evaluation of the ventricular flow alteration in presence of mitral valve stenosis. The model is based on the direct numerical simulation of the Navier–Stokes equations two-way coupled with a structural solver for the left ventricle and mitral valve dynamics. The presence of mitral valve stenosis is mimicked by a single-parameter constraint acting on the kinematics of the mitral leaflets.

Four different degrees of mitral valve stenosis are considered focusing on the hemodynamic alterations occurring in pathologic conditions. The mitral jet, generated during diastole, is seen to shrink and strengthen when the stenosis gets more severe. As a consequence, the kinetic energy of the flow, the tissues shear stresses, the transvalvular pressure drop and mitral regurgitation increase. It results that, as the stenosis severity level increases, the geometric and effective orifice areas decrease up to 50% with respect the normal case due to the reduced leaflets mobility and stronger blood acceleration during the diastolic phase. The modified intraventricular hemodynamics is also related to a stronger pressure gradient that, for severe stenosis, can be more than ten times larger than the healthy valve case. These computational results are fully consistent with the available clinical literature and open the way to the virtual assessment of surgical procedures and to the evaluation of prosthetic devices.

1. Introduction

Mitral valve stenosis is a pathological condition in which the mobility of the valve leaflets is reduced typically because of calcification (Runge et al., 2010). As a consequence the valve does not open properly, thus altering the blood flow from the left atrium to the left ventricle and, in turn, decreasing the heart pumping efficiency. Generally, the less the valve opens, the more the blood flow is impeded, and the more severe is the disorder. The abnormal valvular losses cause a pressure increase in the left atrium in turn inducing atrial–wall thickening and often atrium dilatation. The augmented atrial pressure may also produce blood congestion in the pulmonary veins: in severe stenoses the effect can extend to the lungs and even to the right ventricle of the heart, resulting in the so–called pulmonary hypertension.

Depending on the consequences of the stenosis, different treatment procedures are available. In case of mild stenosis, drug therapies based on diuretics and anticoagulation medications are typically used to relieve patient's discomfort. On the other hand, more severe stenoses call for surgical intervention such as (i) valvuloplasty, (ii) valve repair and (iii) valve replacement. The first one consists of inserting from the leg a thin catheter through the femoral artery and the aorta and placing its tip at the mitral valve opening. From the catheter tip, a balloon is then inflated, which stretches the narrowed valve and widens its lumen. An open heart surgery, such as valvotomy, is instead needed to shave back the leaflet edges when they have become scarred and fused together. In the most severe cases, the mitral valve is replaced by a prosthesis, either mechanical or biological, depending on the patient age and lifestyle (Meschini et al., 2018a).

Among the available therapies the cardiac surgeon selects the most suitable not only according to the specific patient pathology but also considering his experience and the available clinical data. In this sense, computational engineering is becoming an added

* Corresponding author.
E-mail address: f.viola@utwente.nl (F. Viola).

https://doi.org/10.1016/j.jbiomech.2019.01.002
0021-9290/

value in medical research since it provides more details on heart pathologies and can predict the most favorable medical treatment. Numerical simulations, in fact, allow to test and compare new prostheses and surgical procedures and yield a complete access to hemodynamics data, which are unattainable by *in-vivo* experiments. On the other hand, a computational model yields a high-fidelity representation of the ventricular hemodynamics only when all the main features of the system are properly considered. In this framework, different computational models have been proposed to study the aortic and mitral valves of the left ventricle. Concerning the aortic valve stenosis, several studies can be found in which a fluid–structure interaction algorithm is employed to assess the severity of the stenosis (Van Loon, 2010; Bahraseman et al., 2016; Amindari et al., 2017). On the contrary for the mitral valve less studies are available (see Binder et al., 2000; Bluestein and Einav, 1995; Baumgartner et al., 2009; Wunderlich et al., 2013 among others) and none of them relying on computational modeling.

In order to fill this gap, we present a numerical approach to model the mitral valve stenosis and to investigate its effects on the left-ventricle hemodynamics. Both the mitral leaflets and the left-ventricle dynamics are two-way coupled with the blood flow through a full fluid/structure interaction approach. The resulting dynamics of the whole system is then investigated in physiological and pathological conditions to highlight the alterations of the ventricular flow produced by the mitral valve stenosis. Here, the severity of the stenosis is progressively increased from moderate to acute according to the current risk stratification (Zoghbi et al., 2003). The results are then discussed in terms of the clinical parameters commonly used to assess valve stenosis such as the geometric orifice area (GOA), the effective orifice area (EOA) and the transvalvular pressure drop (TPD).

The paper is structured as follows. In the next section the problem configuration and the numerical method, along with the model for the stenotic mitral valve are introduced. The results for the various levels of mitral valve stenosis are then presented and compared against the healthy valve configuration in Section 3. The closing remarks and the perspectives for future studies are given in the final section.

2. Materials and methods

2.1. Problem configuration and mitral stenosis modelling

The main features of the computational framework are sketched in Fig. 1. The mitral valve is made of an anterior (red[1]) and a posterior (blue) leaflet that are modeled as deformable membranes 1 mm thick and are positioned inside a deformable left ventricle with end-systolic volume of 50 ml and thickness 8 mm. These bodies are then anchored to a rigid valvular plane (the fibrous trine) that embeds two rigid pipes of inner diameter 24 mm and 19 mm. The first is placed above the mitral valve and allows the blood to flow into the left ventricle through the valve. The second pipe models the initial tract of the aorta. Since the focus of this work is on the mitral valve kinematics, in order to reduce the computational load, the aortic valve has been replaced by a porous disk placed within the aortic channel with a time-dependent porosity (de Tullio et al., 2011). During diastole, the medium permeability goes to zero, thus closing the duct and preventing the fluid from leaving the ventricle. During systole, in contrast, the permeability tends to infinity and blood can flow through the aortic channel to enter the aorta. The three-dimensional geometries are not patient-specific but instead they have been built using modeling softwares, reference dimensions and shapes extracted from large databases of clinical images available from the literature and medical atlas (Runge et al., 2010). We wish to stress that in the present model all the complex boundaries are handled within an immersed boundary approach therefore either standard– and patient–specific geometries can be simulated within the same ease and efficiency. In this paper however, we have decided to focus on the former set–up in order to highlight the general behaviour of the phenomena rather than characterizing a specific patient.

The reference frame is as shown in Fig. 1, with the positive z-axis pointing vertically downward (parallel to the mitral valve axis) and the $y = 0$ plane is the symmetry plane for the system.

Pathologic mitral valve conditions are modeled by a geometrical constraint on the leaflet kinematics. In order to replicate the reduced mobility of the mitral leaflets due to calcification, a certain portion of the leaflets close to the roots is blocked to a fixed position. The stenosis severity is controlled by varying the vertical extension of the penalization region up to a certain value z_s; larger z_s correspond to more severe stenosis. Specifically, four stenosis levels have been considered here: first $z_s = 0.1d^*$, second $z_s = 0.2d^*$, third $z_s = 0.3d^*$ and fourth $z_s = 0.4d^*$, where d^* is the diameter of the mitral annulus (here equal to $d^* = 2.4$ cm). Additionally, to better ascertain pathologic effects on the hemodynamics, the non-stenotic case, which corresponds to $z_p = 0$, is also considered. We anticipate that this numerical model for the mitral valve stenosis is found to correctly reproduce the narrowed mitral orifice observed in pathologic conditions.

The contraction/relaxation cycle of the ventricle is driven by imposing an inflow (outflow) on the ventricle through the mitral (aortic) channel according to the physiologic conditions that is shown in Fig. 1(b) as a function of time normalized by the beating period, t/T. In the inflow phase, which corresponds to the diastole, two peaks in the flow-rate are observed. The first corresponds to the rapid passive filling of the ventricle (E-wave), whereas the second is due to the active contraction of the atrium (A-wave) that occurs after the diastasis.

The flow–rate curve considered for this study is obtained for an ejection fraction $EF = 60\%$ and it corresponds to an end-diastolic volume of 125 ml.

2.2. Numerical method

In order to capture correctly the contraction/relaxation of the left-ventricle and the opening/closing of the mitral valve, a fluid–structure interaction strategy is used as in Meschini et al. (2018a). This computational framework has been extensively discussed and validated through a series of studies (see de Tullio and Pascazio, 2016; Spandan et al., 2017 among others), and it is only summarized here.

2.2.1. Fluid solver

The blood velocity, $\mathbf{u}$, and pressure p are governed by the incompressible Navier-Stokes equations, which in non-dimensional form read:

$$\frac{\partial \mathbf{u}}{\partial t} + \mathbf{u}\cdot\nabla\mathbf{u} = -\nabla p + \frac{1}{Re}\nabla^2\mathbf{u} + \mathbf{f}, \qquad \nabla\cdot\mathbf{u} = 0. \tag{1}$$

The Reynolds number, Re, is defined by the mitral valve annulus, $d^* = 2.4$ cm, the maximum inflow velocity during the diastolic phase, U_m^*, and the blood viscosity $\nu = 4.8\times10^{-6}$ m^2 s^{-1}. For a heart pulsating at 60 beats per minute with an ejection fraction $EF = 60\%$, the reference velocity is about $U_m^* = 0.85$ m s^{-1}, which corresponds to $Re = U_m^* d^*/\nu = 4250$. The blood has been considered as a

[1] For interpretation of color in Figs. 1 and 6, the reader is referred to the web version of this article.

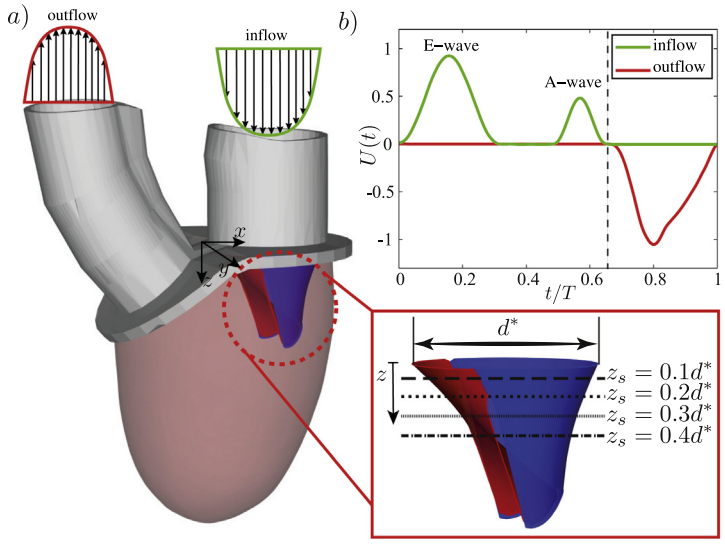

Fig. 1. (a) Visualization of the numerical set-up. The hemodynamics is solved within the left-ventricle, which deforms due to the inflow/outflow flow rates imposed at the mitral and aortic channels that are reported in (b). The inset details the reduced mobility regions of the mitral valve leaflets according to the stenosis model. Each value of the control parameter z_s corresponds to a different stenotic condition that has been here investigated.

Newtonian fluid since it is known that its non-Newtonian features become relevant only in vessels of sub-millimeter diameter (Siginer et al., 1999; Meschini et al., 2018a). Eq. (1) are discretized using the Navier-Stokes solver AFiD Afid http://www.afid.eu, which incorporates an immersed boundary technique (IB) based on a moving least square approach (Vanella and Balaras, 2009). As typical in IB, the no-slip boundary condition on the velocity at the various fluid/structure interfaces is thus imposed by means of the body force f in Eq. (1).

2.2.2. Structural solver

The structural solver consists of a spring–mass model based on an interaction potential approach, Fedosov (2010), de Tullio and Pascazio (2016), Spandan et al. (2017). The immersed surfaces, such as the valve leaflets and the ventricle, are discretized by using triangular meshes whose vertices are connected by ideal elastic springs. The total mass of the body is uniformly distributed among its vertices. Each deformable body thus results in a complex network of vertices that deforms by means of external forces (hydrodynamics loads) and internal potential energy, which include elastic energy, bending energy, area and volume energy that are stored into the deforming bodies. In particular, the elastic and bending energies are computed using the expressions from the Van Gelder model, Gelder (1998), valid in the limit of isotropic membranes. The spatial gradient of the potentials provides the internal forces applied to the body vertices. The internal and external forces acting on each vertex have to balance its inertia, according the second Newton's law. The latter is readily integrated twice in time for any node, thus obtaining the instantaneous configuration of the structure at each time step.

We wish to stress that the fluid dynamics loads come directly from the integration over the tissue/fluid interface of the pressure and viscous stresses therefore there are no additional models or empirical parameters. Since the valve leaflets are deformable membranes, an important component of the structural solver is the contact model that has to cope with the leaflet coaptation along arbitrary surfaces in space. The model consists of two main ingredients: the contact detection module and the kinematic/dynamic laws of the contact. In the former, a three-dimensional integer array is defined with an element for each Eulerian fluid cell; the array is null in the fluid phase and is set to a different integer value for each structural element (for example 1 for the ventricle, 2 for the anterior mitral leaflet, 3 for the posterior one, etc.). Whenever a node of a moving body enters an Eulerian cell tagged by a non null value, the kinematic/dynamic module is invoked that imposes the prescribed rules. In this study we have imposed that if two triangles from different structures happen to be in the same cell, they move together with their averaged velocity if the relative velocity is negative and no conditions are applied otherwise. This prevents the mitral valve leaflets from compenetrating during the systolic phase and to freely open during the diastole. In the case a triangle of the leaflet ends up in a cell occupied by the ventricle, their velocities are reversed so that the leaflet rebounds away from the ventricle. This simple contact model for the mitral leaflets yields perfect valve closure without prescribing a coaptation zone and, at the same time, prevents the moving bodies from piercing each other. Further details and validations for this model, including dynamics contact conditions are available in the literature (Spandan et al., 2018).

In the real heart, once the mitral valve is fully closed the *cordae tendineae*, which connect the leaflets tips to the ventricle wall via the papillary muscles (Meschini et al., 2018b), prevent the valve from prolapsing into the atrium. Here this constrain is mimicked by simple kinematic conditions that freeze the vertical (z) coordinate of the triangular leaflets elements, during the systole, once the valve is sealed.

2.2.3. Two-way fluid-structure coupling and numerical convergence

The model has both 'strong' and 'loose' coupling modes for fluid and structure in order to be able to cope at the same time with inertia–dominated and added-mass-dominated structures. After an extensive series of preliminary simulations, convergence checks and validations (see Meschini et al., 2016; Meschini et al., 2018b), it was determined that the loose-coupling yields the same results as the strong counterpart provided a time sub-stepping procedure is adopted for the structure solver in order to maintain the system stable. Typically a strong-coupling approach needs 4–5 iterations between the flow and structure while a loose-coupling with structure substepping requires a single call to the flow solver and 10–100 calls to the structure module. Since the latter takes only few percents of the computational time with respect to the fluid we have found more convenient the loose coupling-approach. It is

worthwhile to note that this is true for the present problem since the fluid mesh has an order of 2.4×10^6 nodes while the structure has in total less than 4×10^4 triangles; in problems where the structural solvers has to handle larger meshes the same computational approach might be unfavorable and a strong coupling would be preferable. Finally, the number of structural substeps is strongly dependent on the tissue/fluid density ratio; when this ratio is order one or bigger a loose coupling approach is still possible, in contrast for ratios smaller than one the loose coupling approach is unstable regardless of the number of substeps.

At each time-step, the flow field is solved and the corresponding hydrodynamic loads are then used, together with the internal forces, to integrate the vertices displacements. The updated structural configuration is stored and given as input to the flow solver for the successive time-step.

The governing Eq. (1) are solved over a cartesian mesh made by 129^3 nodes evenly distributed in all three directions. This computational domain embeds a left-ventricle that is discretized by 3×10^4 triangles and the two mitral leaflets with 8×10^3 triangles in total. In such a way, the ratio between the Lagrangian (triangle) resolution and the local Eulerian grid spacing is about 0.77, which ensures the correct enforcement the no-slip boundary condition on the bodies (de Tullio and Pascazio, 2016). A dynamic time-step formula that provides a constant Courant number $CFL = 0.2$ is used for time integration. The integration is performed over 11 heart beats and, by monitoring the time evolution of the flow energy, a quasi–periodic regime is attained after the first cycle. As a consequence, phase–averaged quantities are computed using the last 10 heart beats (thus discarding the first one).

This numerical method and grid resolution have been shown to correctly capture ventricle and valves dynamics. We refer to Meschini et al. (2018a) for a careful grid independence study and to Meschini et al. (2018a,b) for two different validations against experiments concerning both the ventricular flow and the dynamics of the mitral leaflets: despite some differences due to cycle-to-cycle variations and small scales dynamics, a good matching between experimental measurements and numerical results is observed.

3. Results

3.1. Ventricular hemodynamics

In this section we investigate how mitral valve stenosis affects the ventricular hemodynamics and the leaflets dynamics. Fig. 2 shows the velocity vectors superimposed on isolevels of the vertical velocity in the $x - z$ symmetry plane in healthy and pathologic conditions. In the normal valve case (first row), during early diastole, the E-wave accelerates the flow through the mitral orifice, thus opening the valve and producing a strong mitral jet. This jet is directed towards the ventricle lateral wall owing to the asymmetry of the leaflets. As the peak of the E-wave is attained, the leaflets open wider, the jet points vertically down to the ventricle apex and a strong recirculation is generated. After the initial passive filling has slowed down then diastasis starts and the vortex on the posterior side of the mitral valve completely vanishes while the other on the anterior side continues to grow. The flow rearranges into a single large structure, that is a vortex occupying the whole ventricle and moving from the apex upwards to the aortic channel, in agreement with previous in vivo (Eriksson et al., 2010) and in vitro (Fortini et al., 2013) experiments. Then, another fluid injection is generated by the A-wave, generating a flow dynamics similar to the one produced by the E-wave, but weaker, which further reinforces the large-scale vortex and keeps the recirculation alive during the whole diastole as visible in Fig. 2 (central column) and also observed in Govindarajan et al. (2018). As systole starts, the pressure in the ventricle increases and an incipient regurgitation is observed through the mitral channel; this minimal back–flow is needed to close the mitral leaflets that, once sealed, allow the blood to leave the ventricle only through the aortic channel. At the end of the systole, the initial configuration is recovered and the cardiac cycle repeats itself. Although a similar flow dynamics is observed for moderate valve stenosis (second row in Fig. 2), significant differences are present. The mitral jet is shrunk during the E-wave because of the reduced mobility of the valve leaflets producing a core with higher velocity and stronger shear layers at the edge that are evidenced by a more irregular structure. These features are exacerbated in the acute stenotic case (third row) where the mitral jet is the narrowest and also bent towards the ventricle wall.

Another important difference is the increase of the mitral regurgitation during systole that will be discussed in detail in the next section. The altered dynamics is also visible in Fig. 3 where the kinetic energy of the flow integrated over the ventricle is shown. Since the blood flow rate is prescribed (see Fig. 1) a similar time evolution is observed for all cases with a first peak at $t/T = 0.2$, produced by the E-wave, followed by a decay during the diastasis ($0.3 \leqslant t/T \leqslant 0.5$). A second smaller peak due to the A-wave ($t/T = 0.56$) closes the filling part of the cycle. During the systole ($0.65 \leqslant t/T \leqslant 0.71$) the flow kinetic energy increases again owing to the intense velocities in the region around the aortic channel. The sudden energy drop at $t/T = 0.78$ indicates the fast closure of the mitral valve that prevents the continuous blood regurgitation towards the left atrium and allows the blood flow through the aorta only. In general, for more severe stenosis levels higher values of kinetic energy are observed, especially during E-wave and A-wave peaks. In fact the smaller mitral orifice area yields faster jets that, however, are not beneficial for the ventricular flow because they are associated with stronger turbulent fluctuations and larger transvalvular pressure drops both concurring to yield a reduced ventricular recirculation.

3.2. Mitral leaflets dynamics

These significant flow changes observed during diastole originate from the reduced mobility of the valve leaflets. In order highlight the abnormal leaflet dynamics, Fig. 4 shows the coordinates of the centroid of the posterior (x_p-z_p) and anterior (x_a-z_a) leaflets. All quantities have been phase-averaged over ten heart cycles. Owing to its physiological reduced mobility, the posterior leaflet is not strongly affected by the stenosis as both x_p and z_p maintain a similar behaviour when the stenosis level is progressively increased (Fig. 4(a), (b)). The dynamics of the anterior leaflet, in contrast, is strongly affected by the stenosis (Fig. 4(c), (d)): the x_a and z_a displacements are significantly inhibited as the stenosis becomes more severe. This reduced motion has a crucial role in the valve closure because it prevents the leaflets from sealing thus yielding an abnormal reflux from the ventricle through the mitral channel (mitral regurgitation). This is also visible in the top part of Fig. 6 where the valve configuration corresponding to the maximum opening is shown in normal and pathologic conditions: the posterior leaflet (blue) is weakly affected by the stenosis whereas the anterior leaflet (red) flapping is significantly reduced.

As mentioned above, the reduced mobility of the mitral leaflets causes during systole an incomplete valve closure that is responsible for blood regurgitation that increases with the stenosis severity: the regurgitant blood volume from the numerical results turned out to be, 5.07, 9.34, 16.09 and 33.68 ml, respectively for the stenosis levels from 1 to 4. These values correspond to 6.76%, 12.45%, 21.40% and 45.00% of the total ejected volume to be com-

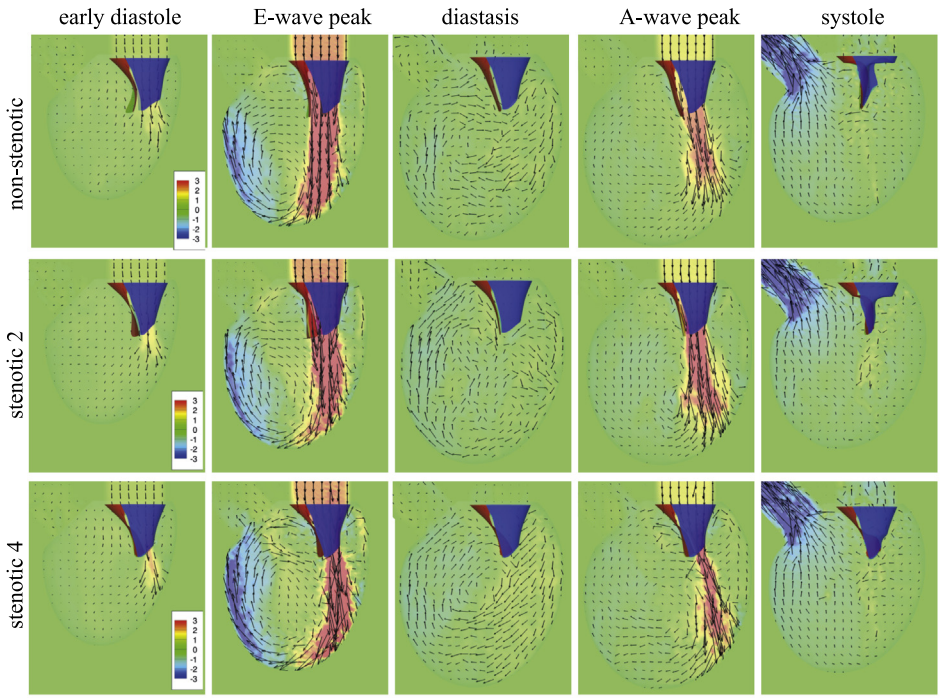

Fig. 2. Instantaneous snapshots of the nondimensional velocity vectors in the $x-z$ symmetry plane and contours of the vertical velocity over the cardiac cycle. The normal valve condition ($z_s = 0$) is depicted in the first row, whereas stenotic 2 ($z_s = 0.2$) and stenotic 4 ($z_s = 0.4$) cases are shown in the second and third row.

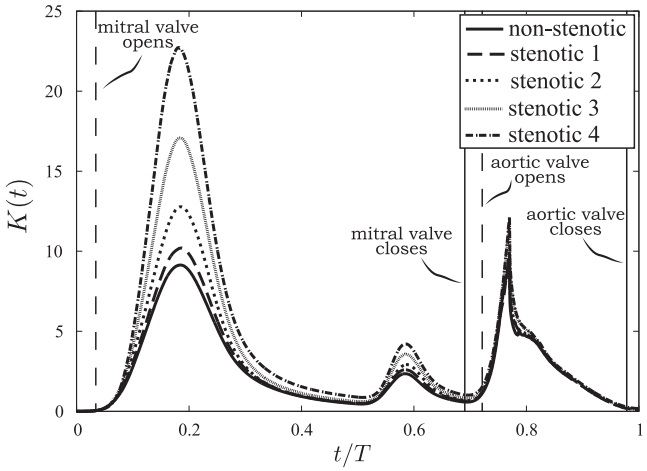

Fig. 3. Phase-averaged (over ten heart beats) kinetic energy of the flow integrated over the left-ventricle domain as a function of time normalized by the heart beating period.

pared with 5.33% (4.00 ml) of the physiological healthy case. It is worthwhile to mention that, while these values are consistent with the clinical data from the literature, they should be taken with care since the inflow/outflow conditions of the present model are different from those of the heart whose pressure difference between left atrium and ventricle determines the mitral regurgitation.

3.3. Tissues shear stress

Within the computational framework is also possible to study how the mitral valve stenosis affects the wall shear stresses (WSS). In order to further investigate the effect of the modified mitral jet due to valve stenosis, Fig. 5 shows the WSS modulus experienced by the mitral valve leaflets and the ventricle averaged during diastole. In the non-stenotic case (a, b) the highest WSS over the leaflets is observed at their tips where the shear layers detach merging in the mitral jet (see the E-wave snapshot in Fig. 2). Owing to their triangular geometry, the lower tips of the anterior leaflets correspond to the locations of higher WSS, which is about twice the maximum WSS in the myocardium. The latter is less intense at the ventricle basis, while it increases significantly moving towards the apex where the mitral jet impinges violently on the myocardium as visible in Fig. 5(c).

For moderate stenosis (Fig. 5(d), (e), (f)) the valve leaflets undergo a more intense WSS that spreads over the leaflets surface. This observation can be rationalized recalling that, even if the flow moving through the valve accelerates due to the reduced leaflets mobility, the no-slip boundary condition at their surface still has to be respected. As a results, high velocity gradients at the leaflets walls, which are proportional to the WSS, take place. Furthermore, the resulting mitral jet has an high velocity core and strong shear layers, which then impact on the myocardium thus inducing higher WSS to increase in the stenotic case, as depicted in Fig. 5 (f). This scenario is further exacerbated in the case of severe mitral valve stenosis reported in Fig. 5(g), (h), (i). The high WSS region extends to the lower half of the posterior leaflet and covers almost the whole surface of the anterior one. Also the WSS in the myocardium further increases for stenotic case 4 and a large region of high WSS emerges. It has to be remarked that the average WSS at the apical region for acute stenosis is significantly larger than the maximum WSS observed for the healthy case (Fig. 5(c)).

3.4. Clinical parameters for valve stenosis

In this section the proposed computational framework is employed to estimate some relevant parameters that are commonly used in clinical applications to quantify mitral valve stenosis.

3.4.1. Geometric orifice area (GOA)

The GOA is defined as the area delimited by the leaflets edges when observed from the mitral channel direction. This quantity

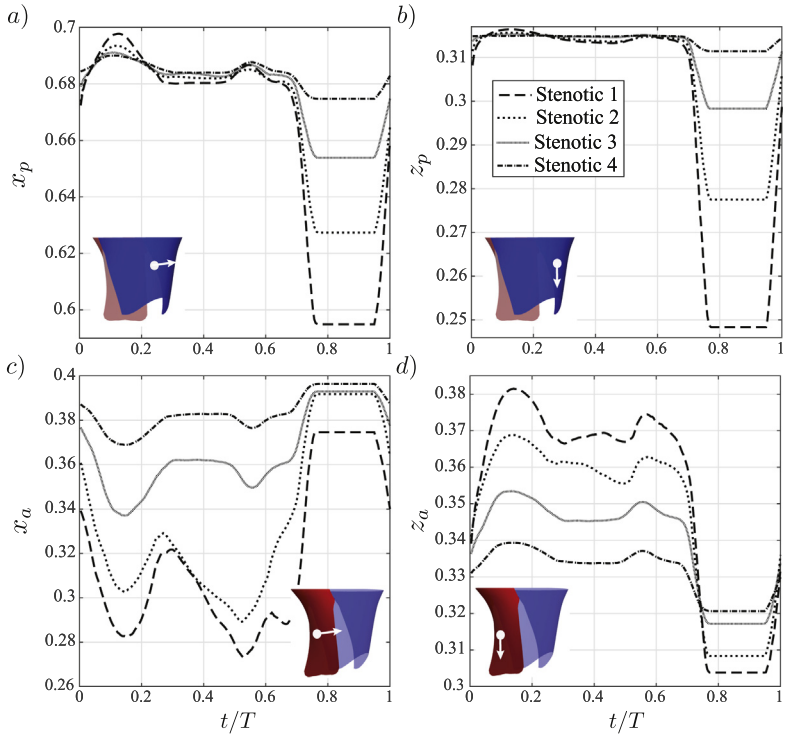

Fig. 4. Dynamics of the posterior and anterior mitral leaflets for the four stenotic conditions studied. Mean (a) horizontal, x_p, and (b) vertical, z_p, motion of the posterior leaflet, along with mean (c) horizontal, x_a, and (d) vertical, z_a, motion of the anterior leaflet. All quantities have been phase-averaged over ten cardiac cycles.

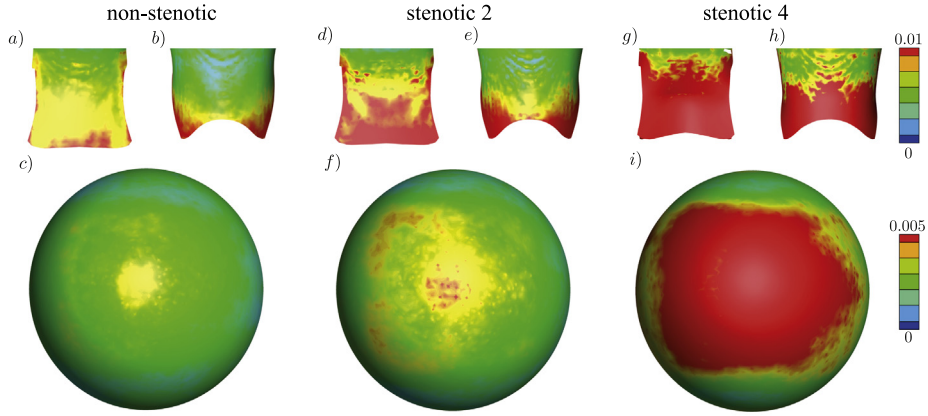

Fig. 5. WSS modulus averaged during one diastole on the (a) anterior leaflet, (b) posterior leaflet and (c) LV (bottom view) for the non-stenotic mitral valve. The same quantity is shown for stenotic configurations: (d, e, f) stenotic 2 and (g, h, i) stenotic 4. The instantaneous WSS is the vector defined as $\tau = S_\tau \mathbf{n}$, where S_τ is the off-diagonal part of the stress tensor and $\mathbf{n}$ is the local normal vector.

is purely geometric because it does not provide any direct information about the flow features. The time evolution of GOA phase averaged over ten cardiac cycle, both in healthy and stenotic conditions, is shown in Fig. 6. As expected, all over the cardiac cycle it is found that more severe stenoses yield smaller GOAs. In the most severe stenosis case (stenotic 4) the maximum orifice area, at the peak of the E–wave, is reduced by almost 60% with respect to the non-stenotic mitral valve simulations. It is worth noticing that in the non-stenotic case the GOA is about zero during systole ($0.8 < t/T < 1$) implying that, in physiological conditions, the mitral leaflets are sealed and a perfect valve closure is ensured. In contrast, for the stenotic cases the mitral leaflets do not line up, due to their reduced mobility, and the GOA is non–zero during systole. This imperfect closure becomes more pronounced as the stenosis severity level increases and, for the most severe case, it can be as large as $GOA = 0.2\ \mathrm{cm}^2$, which corresponds to about 20% of the maximum GOA measured at E-wave peak. In medical terms this results in the mitral regurgitation that produces an abnormal reflux from the left ventricle to the left atrium during systole.

3.4.2. Effective orifice area (EOA)

A more effective quantity to assess valve performance is the EOA. The latter is defined as the ratio of the peak flow rate through the mitral valve, Q_{max}, to the maximum velocity over the mitral jet, V_{max}:

$$EOA = \frac{Q_{max}}{V_{max}}. \tag{2}$$

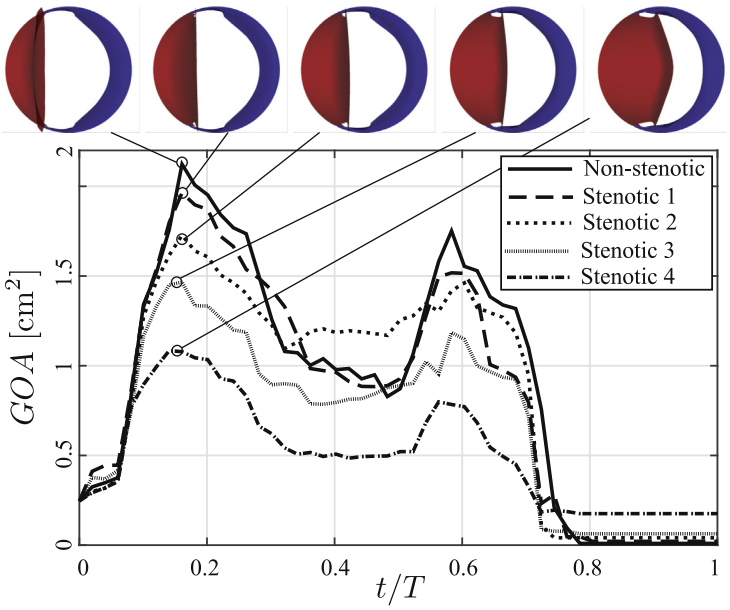

Fig. 6. Time evolution over a cardiac cycle of the values of the GOA. The top figure shows the mitral valve configurations corresponding to the maximum GOA (bottom view). All quantities have been phase-averaged over ten cardiac cycles.

As a results, the EOA, is a measure of the blood displacement through the mitral valve that characterizes better the severity of the stenosis compared to GOA. Please note as other similar, but not strictly equivalent, definitions of the EOA are used in the literature depending on the application and on the measurements technique, see (Baumgartner et al., 1992; Garcia et al., 2012) for a comprehensive discussion. As evident in Table 1, EOA is smaller than the E-wave GOA both in normal and pathological conditions. This is readily explained by recalling that EOA corresponds to the minimum cross section of the blood streamtube across the mitral jet. According to the *vena contracta* phenomena, the maximum jet restriction typically occurs slightly downstream of the mitral orifice (where the GOA is measured) and the EOA is smaller than the GOA.

As shown in Table 1, the effect of the stenosis level on EOA is similar to that of GOA since also the former decreases monotonically and, in the most acute stenosis case, (stenotic 4) it is about half the value measured in physiological conditions.

3.4.3. Transvalvular pressure drop (TPD)

Another important parameter that is typically employed to assess the severity of the stenosis is the TPD. This quantity is defined as the pressure difference across the valve, as in Fig. 7(a), and depends not only on the valve geometry and on the continuity equation, but also on the balance of momentum in the flow. TPD values below 2.5 mmHg are generally associated to physiological condition, whereas $2.5\ \mathrm{mmHg} \leqslant \mathrm{TPD} < 5\ \mathrm{mmHg}$ and $5\ \mathrm{mmHg} \leqslant \mathrm{TPD} < 10\ \mathrm{mmHg}$ evidence mild and moderate stenosis, respectively. A TPD greater than 10 mmHg indicates a severe stenosis, see (Baumgartner et al., 2009). Fig. 7(b)–(e) shows the instantaneous pressure field at the E-wave peak in physiological and stenotic conditions. In all cases the pressure is negative (with respect the reference pressure) downstream of the mitral valve within the mitral jet. A positive pressure region, which originates from the mitral jet impingement on the myocardium, is visible close to the lateral wall. In the non-stenotic case, these pressure variations are neither intense nor extended in space. On the contrary, when the stenosis increases, the low pressure region progressively spreads at the center of the ventricle whereas the high pressure propagates towards the ventricle apex. In these conditions, the TPD increases with severity of the mitral valve stenosis as reported in Table 1. In particular, the TPD (1.87 mmHg in physiological conditions) increases up to 26.71 mmHg for the most acute stenosis, which would indicate life threatening conditions in the clinical practice.

4. Discussion

4.1. An effective model for mitral valve stenosis

In this paper the effect of mitral valve stenosis on the ventricular flow is studied numerically by a computational tool that can cope simultaneously with the hemodynamics and the deformation of left–ventricle and mitral valve. The system dynamics is obtained by integrating the full Navier-Stokes equations two–way coupled with a structural solver based on an interaction potential approach. This numerical model mimics the mitral valve stenosis by preventing the leaflets mobility in a range of the vertical coordinate $0 \leqslant z \leqslant z_s$; this is the only control parameter and it determines the severity of the pathology, which has been set so to reproduce four different mitral stenoses from mild to acute. The flow in a healthy mitral valve has been also computed in order to evidence the abnormal dynamics when the valve pathology occurs.

In healthy conditions, as the E–wave propagates, the blood flows from the mitral channel into the ventricle, producing a strong mitral jet. As the peak of the E-wave is attained, the leaflets open wider, the jet points vertically down to the ventricle apex and a strong recirculation is generated. After the initial passive filling a second weaker jet is produced by the active contraction of the atrium (A–wave) that sustains the large–scale recirculation throughout the systole. A similar scenario is observed also for a stenotic mitral valve although, during the E–wave, the mitral jet results faster and more irregular due to the reduced mobility of the valve leaflets. These differences in the ventricular flow have important implications on the heart pumping efficiency. In fact a faster mitral jet is not as efficient as the physiological one since, while its maximum velocity is about three times bigger than the reference case, the peak velocity at the ventricle apex results only 15% more intense. Furthermore, the decay rate of the recirculation can be fast enough not to sustain it throughout the systole; for the

Table 1
Model control parameter z_s and corresponding values of maximum GOA, EOA and TPD over a heart beat.

Case	z_s	GOA_{max} [cm^2]	EOA [cm^2]	TPD [mmHg]
Non-stenotic	0.0	2.12	1.51	1.87
Stenotic 1	0.1	1.796	1.40	3.48
Stenotic 2	0.2	1.73	1.28	6.39
Stenotic 3	0.3	1.47	1.03	12.03
Stenotic 4	0.4	1.08	0.78	26.71

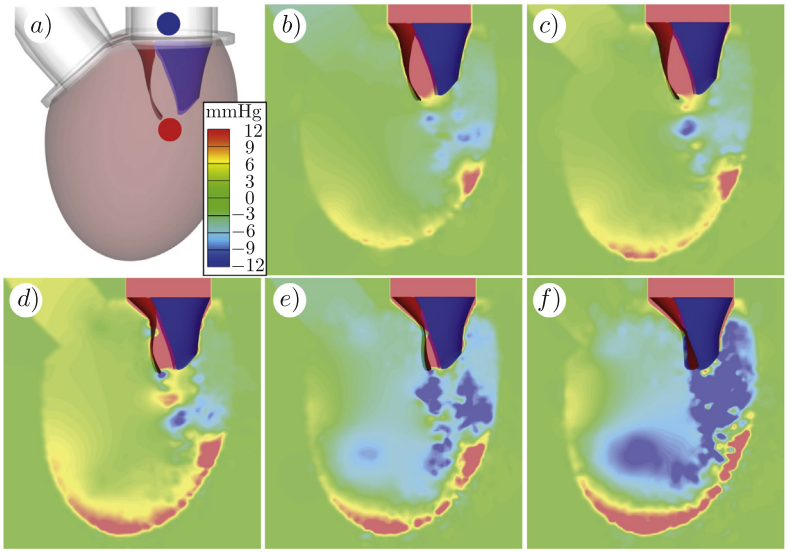

Fig. 7. (a) Reference configuration for the evaluation of the pressure difference values: upvalvular value (blue dot) and subvalvular value (red dot). Instantaneous snapshots of the pressure fields at the peak of the E-wave for the different stenosis severity levels: (b) non-stenotic valve; (c) stenosis up to $z = 0.1$; (d) stenosis up to $z = 0.2$; (e) stenosis up to $z = 0.3$; (f) stenosis up to $z = 0.4$. (For interpretation of the references to color in this figure legend, the reader is referred to the web version of this article.)

most severe stenoses this suppresses the ventricle washout, which is of primary importance for the correct left ventricle functioning. These modified ventricular hemodynamics and valve kinematics also alter the kinetic energy of the flow as well as the WSS, which are found to be positively correlated with the stenosis severity. In particular, the flow acceleration through the stenotic valve yields high velocity gradients and, as a consequence, high shear stress at the leaflets surface. Additionally, the shear layers detaching from the leaflets are very intense and impact on the myocardium along with the concentrated mitral jet thus yielding the myocardium WSS to increase significantly, especially during systole, with respect to the healthy case. Conversely, diastasis is only weakly affected by the valve stenosis and, for all healthy and stenotic configurations, during this phase the flow rearranges into a single large structure occupying the whole ventricle and moving from the apex upwards to the aortic channel. This large vorticity structure is then straightened by the A-wave jet.

In order to further assess the effectiveness of our approach, medical parameters that are commonly used in clinical practice have been monitored for the healthy and pathological cases. It results that as the stenosis severity level increases the GOA decreases due to the reduced leaflets mobility. A smaller GOA then yields a stronger blood acceleration during the diastolic phase, which, in turn, narrows the blood streamtube through the valve and, concurrently, decreases the EOA. In the most severe case (stenotic 4) both, GOA and EOA decrease by 50% with respect the normal case. Furthermore, a more intense blood acceleration is related to a stronger pressure gradient. Hence, the pressure difference between the mitral channel and the ventricle increases significantly; it ranges from the physiological value of $TPD = 1.87$ mmHg to the abnormal level of $TPD = 26.87$ mmHg, for the most severe stenosis. These computed parameters turn out to be in the range of those obtained by *in vivo* clinical diagnostics.

In a nutshell, the model not only predicts the correct trends for EOA, GOA and TPD when the stenosis severity level increases but also provides data which are consistent with the clinical experience.

4.2. Limitations

Despite the computational effort in making the model as close as possible to the intended application some aspects still need to be addressed. The first possible improvement could be to consider a non-uniform thickness distribution for the valve leaflets, which is known to be generally different between anterior and posterior (May-Newman and Yin, 1998) and to depend and the specific valve location (Sahasakul et al., 1988). Furthermore the tissue thickness varies significantly on the age: due to thickening and degeneration of collagen fibers and to lipid accumulation and calcification, the leaflet thickness increases with aging. Sahasakul et al. (1988) observed that, for the thickest size on each leaflet, the mean thickness among subjects aged $\geqslant$ 60 years old is about twice that for those between 20 and 59 years old. In particular, the anterior leaflets the maximum thickness increases from 1.60 mm to 3.20 mm, whereas a thickening from 1.13 mm to 2.04 mm happens for the posterior one. In general calcification can be more intense on one leaflet and the non-uniform thickness distribution may indeed affect the valve kinematics and, as a consequence, the intraventricular hemodynamics. However, due to the great variability among individuals (especially due to the age) in order to properly account for the effect of the leaflets' thickness and differential calcification would require an extensive simulation campaign, which is beyond

the scope of this work that focuses on the reduced leaflets mobility induced by the valve stenosis. To this aim, we have modeled the valve as 1 mm uniformly thick media, which is a reasonable value according to the literature. Additionally, the effect of the chordae tendineae has been modeled here by simple kinematic conditions that prevent the mitral leaflets from everting inside the mitral channel. Although they do not affect particularly the global flow dynamics, they can be included in our computational model, as proposed by Meschini et al. (2018b), to further increase the model accuracy.

Another difference is that in our model the mitral annulus is assumed to be planar and rigid, while in biological conditions its shape changes during the heartbeat and is flat during diastole then becoming saddle shaped during systole (Levine et al., 1987; Salgo et al., 2002; Votta et al., 2008). Hence, this annulus non-planarity mainly affects the mobility of the posterior leaflet and facilitates the valve closure during systole (Levine et al., 1987; Salgo et al., 2002). In this paper, however, we are mainly concerned with the diastolic phase when the mitral valve opens and the ventricular flow is generated, thus we expect this feature of annulus planarity not to significantly affect our conclusions.

A last important advancement for the computational model would be to replace the prescribed inflow/outflow condition with an active contraction/relaxation of the left ventricle. This step could be done by including in the fluid-structure interaction algorithm an electrophysiology model responsible for the propagation of the electrical stimulus through the wall ventricle. As a result, the ejection fraction would be a function of the pathology degree rather than a prescribed parameter. Such approach, which is an ongoing work of the authors, would increase the model reality and would make it more suitable for clinical applications.

Conflict of interest

None.

Acknowledgements

F.V. acknowledges the support of the Swiss National Science Foundation (Grant No. P2ELP2_172320).

References

Afid www.afid.eu.
Amindari, A., Saltik, L., Kirkkopru, K., Yacoub, M., Yalcin, H.C., 2017. Assessment of calcified aortic valve leaflet deformations and blood flow dynamics using fluid-structure interaction modeling. Inform. Med. Unlocked 9, 191–199.
Bahraseman, H.G., Languri, E.M., Yahyapourjalaly, N., Espino, D.M., 2016. Fluid-Structure Interaction modeling of aortic valve stenosis at different heart rates. Acta Bioeng. Biomech. 18 (3).
Baumgartner, H., Khan, S.S., DeRobertis, M., Czer, L.S., Maurer, G., 1992. Doppler assessment of prosthetic valve orifice area. An in vitro study. Circulation 85 (6), 2275–2283.
Baumgartner, H., Hung, J., Bermejo, J., Chambers, J.B., Evangelista, A., Griffin, B.P., Iung, B., Otto, C.M., Pellikka, P.A., Quinones, M., 2009. Echocardiographic assessment of valve stenosis: EAE/ASE recommendations for clinical practice. J. Am. Soc. Echocardiogr. 22 (1), 1–23.
Baumgartner, H., Hung, J., Bermejo, J., Chambers, J.B., Evangelista, A., Griffin, B.P., Iung, B., Otto, C.M., Pellikka, P.A., Quiones, M., 2009. Echocardiographic assessment of valve stenosis: EAE/ASE recommendations for clinical practice. J. Am. Soc. Echocardiogr. 22 (1), 1–23.
Binder, T.M., Rosenhek, R., Porenta, G., Maurer, G., Baumgartner, H., 2000. Improved assessment of mitral valve stenosis by volumetric real-time three-dimensional echocardiography. J. Am. Coll. Cardiol. 36 (4), 1355–1361.
Bluestein, D., Einav, S., 1995. The effect of varying degrees of stenosis on the characteristics of turbulent pulsatile flow through heart valves. J. Biomech. 28 (8), 915–924.
de Tullio, M.D., Pascazio, G., 2016. A moving-least-squares immersed boundary method for simulating the fluid-structure interaction of elastic bodies with arbitrary thickness. J. Comput. Phys. 325, 201–225.
de Tullio, M.D., Pedrizzetti, G., Verzicco, R., 2011. On the effect of aortic root geometry on the coronary entry-flow after a bileaflet mechanical heart valve implant: a numerical study. Acta Mech. 216 (1–4), 147–163.
Eriksson, J., Carlhll, C.J., Dyverfeldt, P., Engvall, J., Bolger, A.F., Ebbers, T., 2010. Semi-automatic quantification of 4D left ventricular blood flow. J. Cardiovasc. Magn. Reson. 12 (9), 1–10.
Fedosov, D.A., 2010. Multiscale Modelling of Blood Flow and soft Matter (Ph.D. thesis). Brown University, Providence, United States.
Fortini, S., Querzoli, G., Espa, S., Cenedese, A., 2013. Three-dimensional structure of the flow inside the left ventricle of the human heart. Exp. Fluids 54, 1609.
Garcia, J., Marrufo, O.R., Rodriguez, A.O., Larose, E., Pibarot, P., Kadem, L., 2012. Cardiovascular magnetic resonance evaluation of aortic stenosis severity using single plane measurement of effective orifice area. J. Cardiovasc. Magn. Reson. 14 (1), 23.
Gelder, A.V., 1998. Approximate simulation of elastic membranes by triangulated spring meshes. J. Graph. Tools 3 (2), 21–41.
Govindarajan, V., Mousel, J., Udaykumar, H., Vigmostad, S.C., McPherson, D.D., Kim, H., et al., 2018. Synergy between diastolic mitral valve function and left ventricular flow aids in valve closure and blood transport during systole. Sci. Rep. 8 (1), 6187.
Levine, R.A., Triulzi, M.O., Harrigan, P., Weyman, A.E., 1987. The relationship of mitral annular shape to the diagnosis of mitral valve prolapse. Circulation 75, 756–767.
May-Newman, K., Yin, F., 1998. A constitutive law for mitral valve tissue. J. Biomech. Eng. 120, 38–47.
Meschini, V., de Tullio, M.D., Querzoli, G., Verzicco, R., 2016. A computational approach for multi-physics biological flows. ECCOMAS Newslett. (June)
Meschini, V., De Tullio, M.D., Querzoli, G., Verzicco, R., 2018a. Flow structure in healthy and pathological left ventricles with natural and prosthetic mitral valves. J. Fluid Mech. 834, 271–307.
Meschini, V., de Tullio, M.D., Verzicco, R., 2018b. Effects of mitral chordae tendineae on the flow in the left heart ventricle. Eur. Phys. J. E 41 (2), 27. Vancouver.
Runge, M.S., Patterson, C., Stouffer, G.A., Netter, F.H., 2010. Netter's Cardiology. Saunders/Elsevier, Philadelphia.
Sahasakul, Y., Edwards, W.D., Naessens, J.M., Tajik, A.J., 1988. Age-related changes in aortic and mitral valve thickness: implications for two-dimensional echocardiography based on an autopsy study of 200 normal human hearts. Am. J. Cardiol. 62 (7), 424–430.
Salgo, S.I., Gorman, J.H., Gorman, R.C., Jackson, B.M., Bowen, F.W., Plappert, T., Sutton, M.G., Edmundus, L.H., 2002. Effect of annular shape on leaflet curvature in reducing mitral leaflet stress. Circulation 106, 711–717.
Siginer, D.A., De Kee, D., Chhabra, R.P. (Eds.), 1999. Advances in the Flow and Rheology of non-Newtonian Fluids, vol. 8. Elsevier.
Spandan, V., Meschini, V., Ostilla-Monico, R., Lohse, D., Querzoli, G., de Tullio, M.D., Verzicco, R., 2017. A parallel interaction potential approach coupled with the immersed boundary method for fully resolved simulations of deformable interfaces and membranes. J. Comput. Phys. 348, 567–590.
Spandan, V., Lohse, D., de Tullio, M.D., Verzicco, R., 2018. A fast moving least squares approximation with adaptive Lagrangian mesh refinement for large scale immersed boundary simulations. arXiv preprint arXiv: 1805.01113.
Vanella, M., Balaras, E., 2009. Short Note: a moving-least-squares reconstruction for embedded-boundary formulations. J. Comput. Phys. 228 (18), 6617–6628. Vancouver.
Van Loon, R., 2010. Towards computational modelling of aortic stenosis. Int. J. Numer. Methods Biomed. Eng. 26 (3–4), 405–420.
Votta, E., Caiani, F., Veronesi, F., Soncini, M., Montevecchi, F.M., Redaelli, A., 2008. Mitral valve finite-element modelling from ultrasound data: a pilot study for a new approach to understand mitral function and clinical scenarios. Phil. Trans. R. Soc. 366, 3411–3434.
Wunderlich, N.C., Beigel, R., Siegel, R.J., 2013. Management of mitral stenosis using 2D and 3D echo-Doppler imaging. JACC: Cardiovascular Imag. 6 (11), 1191–1205.
Zoghbi, W.A., Enriquez-Sarano, M., Foster, E., Grayburn, P.A., Kraft, C.D., Levine, R.A., Nihoyannopoulos, P., Otto, C.M., Quinones, M.A., Rakowski, H., Stewart, W.J., 2003. Recommendations for evaluation of the severity of native valvular regurgitation with two-dimensional and Doppler echocardiography. J. Am. Soc. Echocardiogr. 16 (7), 777–802. Vancouver.